Milsch, H., Kristinsdottir, L. H., Spangenberg, E., Bruhn, D., Flovenz, O. G. (2010): Effect of the water-steam phase transition on the electrical conductivity of porous rocks. - Geothermics, 39, 1, 106-114

DOI: 10.1016/j.geothermics.2009.09.001

GEOT-D-08-00043R3

Effect of the water-steam phase transition on the electrical conductivity of porous rocks

Harald Milsch[1*], Líney H. Kristinsdóttir[2], Erik Spangenberg[1], David Bruhn[1], Ólafur G. Flóvenz[2]

[1]Deutsches GeoForschungsZentrum, Telegrafenberg, 14473 Potsdam, Germany
[2]Icelandic GeoSurvey (ÍSOR), Grensásvegi 9, 108 Reykjavík, Iceland

Manuscript received: 12 November 2008

Abstract

The effect of the water-steam phase transition on electrical conductivity was experimentally investigated in volcanic and sandstone samples to support the interpretation of resistivity data to determine changes in steam saturation in geothermal reservoirs. The measurements were performed at simulated in-situ conditions with controlled pore fluid chemistry, temperature, and confining and pore pressures. At constant temperature (150°C) and confining pressure, pore fluid was withdrawn from the sample by steadily increasing the volume of the pore fluid system. At the vapor saturation pressure, the pore water progressively boiled to steam, resulting in a continuous conductivity decrease by a factor of approximately 20. The study showed that: (1) for rocks in which conduction is controlled by the pore fluid, the concurrent changes in both electrical conductivity and pore (vapour) pressure are defined by the pore size distribution; the changes in liquid-steam saturation are approximately proportional to those in conductivity and can thus be quantified; and (2) for rocks in which surface conduction is predominant there is no direct relation between conductivity, pore pressure and drained fluid volume. This implies that the conduction mechanism controls the pattern of electrical conductivity variations as steam saturation changes.

Keywords: Geothermal; Electrical conductivity; Fluid; Phase transition; Basalts; Sandstones; Iceland

[*] Corresponding author: Tel.: +49 331 288 1527; fax: +49 331 288 1577
E-mail: milsch@gfz-potsdam.de (H. Milsch)

Nomenclature

k	=	temperature constant (MPa/°C)
p	=	pressure (bar)
p_{pore}	=	pore pressure (bar)
p_{boil}	=	pressure at boiling point of water (vapour pressure) (bar)
p_{cap}	=	capillary pressure (bar)
r	=	rate of volume increase in pore fluid pump (µl/min)
R	=	capillary radius (µm)
t	=	time (h)
T	=	temperature (°C)
T_0	=	reference temperature (°C)

Greek symbols

γ	=	surface tension (Pa•m)
θ	=	wetting angle (°)

---

1 bar = 10^5 Pa

1. Introduction

Where pressure in the earth's crust is not high enough to keep water in its liquid phase, boiling starts and steam[1] fills the pore space instead. This may occur when pore pressures decrease in response to the withdrawal of fluids from geothermal reservoirs, particularly in zones that are close to boiling point temperatures and pressures, commonly near the top of these reservoirs.

Because of their high fluid enthalpy, these steam zones (or steam caps) are often well drilling targets and mapping their expansion is therefore essential. Production well enthalpy and pressure measurements directly detect phase changes in the fractures that provide well deliverability. Additionally, there are numerous case histories of the use of precision gravity and geochemistry measurements to characterize steam saturation change in both the fractures and the much larger volume of primary (matrix) porosity (Atkinson and Pederson, 1988; Nicholson, 1993; Hunt and Bowyer, 2007). Repeated conductivity surveys could supplement

[1] Here we treat the terms "steam" and "vapour" as synonyms regardless of whether the gaseous phase contains liquid droplets or not.

such methods. Methods to image the 3D distribution of conductivity in the subsurface to help geothermal development still need improvement; however, advances in noise reduction and mapping techniques are being made. In addition, investigations on the magnitude of conductivity change resulting from pore fluid boiling and related liquid-steam saturation variations, like the one presented here, are valuable for that purpose.

Conduction of electrical current through a volume of porous rock occurs along three pathways: (1) through the rock matrix, (2) with conductive ions in the pore fluid, and (3) along the water-rock interfaces in the pores; see Rink and Schoppers (1976), Guéguen and Palciauskas (1994), and Ruffet et al. (1995) for reviews, and Flóvenz et al. (1985; 2005) for information on Icelandic rocks. The matrix of both the igneous and sedimentary rocks found in geothermal systems is not conductive and so the overall rock conductivity is controlled by pore fluid conduction and interface (surface) conduction. If a dry rock is saturated with distilled water, its conductivity will typically increase by over three orders of magnitude (Duba et al., 1978). In addition, geothermal reservoir water usually contains dissolved ions that increase the fluid conductivity in rough proportion to their concentration. Pores are often lined with clay minerals that adsorb water and ions, causing high surface conductivity.

Many geothermal reservoirs are capped by very conductive, hydrothermally altered clay zones. Although the types of clay found in high-temperature geothermal systems are much less conductive, surface conduction related to clay is often an important component of the bulk conductivity of geothermal reservoir rocks (Boitnott and Hulen, 2001; Flóvenz et al., 2005; Kulenkampff et al., 2005). The relative contribution of pore fluid conduction increases under a variety of conditions, for example in reservoirs with higher pore fluid salinity or with rocks of low clay content.

The overall effect of boiling on electrical conductivity within geothermal reservoirs is poorly constrained by earlier studies although it is expected to decrease once boiling starts.

97 Even though the charge carriers remain in the brine and will enhance the electrical
98 conductivity of the remaining pore water, the increasing amount of electrically isolating steam
99 in the pore network reduces the pathways for the electrical current and, hence, decreases the
100 electrical conductivity. In contrast to this likely scenario for rocks where conductivity is
101 controlled by pore fluid conduction, the direct effect of boiling on surface conduction in the
102 pores remains unknown.

103 Some laboratory measurements of electrical conductivity during vaporization of pore fluid
104 in rock core samples were performed by Roberts et al. (2000; 2001a; 2001b) and Roberts
105 (2002). They studied rocks of different types and porosities, i.e. andesites (11.5 %) and
106 hydrothermal breccias (26.8 %) from Awibengkok (Indonesia); metashales (3.5 ± 1.9 %) from
107 The Geysers geothermal field (USA); and rhyolitic tuffs (9.0 - 13.5 %) from Fran Ridge and
108 Yucca Mountain (USA). Their results showed that pore fluid vaporizes gradually as pressure
109 is decreased and that it occurs at lower pressures than expected from the physical properties of
110 water alone. Based on the Young-Laplace concept of capillarity (e.g. Bear, 1988), this
111 observation led Roberts et al. (2001a) to propose a model for a porous medium, where pore
112 fluid vaporization would be heterogeneous as pore pressure is decreased, because of capillary
113 suction effects. Accordingly, the phase transition occurs first in the largest pores and then in
114 consecutively smaller ones. The consequence is that instead of a sharp decrease in electrical
115 conductivity due to widespread boiling (like that of free water), the conductivity decreases
116 progressively as vapour forms in more and more pores. For a porous medium, vaporization
117 occurs when the pore pressure is:

118 $$p_{pore} \leq p_{boil} + p_{cap}\,, \tag{1}$$

119 where p_{pore}, p_{boil}, and p_{cap} are the pore, boiling (vapour) and capillary pressures, respectively.
120 The capillary pressure, by definition, is negative and inversely related to the radius of the
121 capillary (e.g. Bear, 1988):

$$p_{cap} = -2\gamma \cos\theta / R, \quad (2)$$

where γ and θ are the surface tension of the wetting fluid and the wetting angle, respectively. Therefore, for rocks where conductivity is controlled by pore fluid and not by interface conduction, the resistivity effects due to an increase in steam saturation will strongly depend on the pore microstructure of the reservoir rocks.

A few other studies addressed the effect of steam flooding on the electrical conductivity of unconsolidated sands in the context of enhanced oil recovery and soil remediation (Vaughan et al., 1993; Butler and Knight, 1995). Despite considerable differences in experimental procedures (e.g. non-isothermal conditions) a significant conductivity decrease was observed when steam replaced the saline pore fluid. The extent of this decrease was affected by various factors such as the chemical composition of the fluid (e.g. the salt content) from which the steam was produced, the fraction of vapour within the steam phase (the steam quality), and the injection rate.

In this study, we present the first laboratory measurements of changes in electrical conductivity during pore fluid vaporization for volcanic rock samples from Icelandic geothermal reservoirs. More specifically, the purpose of the present experimental investigation was to monitor the electrical conductivity pattern of a water-steam phase transition and to establish a quantitative relationship between conductivity and steam saturation. In Section 2, the apparatus, the samples, and the fluids used in this investigation are described. Also, an outline of the experimental procedure is given. In Sections 3 and 4, the experimental results are presented and discussed, respectively. Finally, in Section 5, the principal findings of this study are summarized.

2. Experimental setup and procedure

2.1. Apparatus

As in Kristinsdóttir et al. (2007, 2010), the experiments were conducted at the Deutsches GeoForschungsZentrum (GFZ) using a recently installed high-pressure, high-temperature flow-through apparatus. **Figs. 1(a) and (b)** show the general set-up of the apparatus and the mounted specimen assembly, respectively. The apparatus consists of an internally heated oil-medium pressure vessel and a connected pore fluid system. The sample assembly is inserted vertically into the vessel. Both confining and pore pressures are generated with piston-cylinder type syringe pumps. The apparatus allows simultaneous and continuous measurements of permeability, electrical conductivity as well as P- and S-wave velocities.

The electrical conductivity is measured with a four-electrode arrangement and a variable shunt resistor. Two silver rings painted onto the samples with a spacing of 25 mm serve as the potential electrodes. At the current electrodes located on the steel plugs facing the sample, the signals are impressed with a function generator (Agilent 33220A). Typically, the voltage is an AC-sine 1.0 V peak-to-peak signal at a frequency of 13 Hz. The input impedance is 10 MOhms.

The temperature is measured with two PT-100 sensors, one close to the top and one close to the bottom of the specimen, respectively. At 150°C, one notices a temperature difference of approximately 1-2°C along the sample, the topside being the hotter part. A detailed description of the apparatus and specific measurement procedures can be found in Milsch et al. (2008b).

2.2. Samples

The measurements were carried out on four volcanic rock samples from Iceland, two basalts and two hyaloclastites, and one Fontainebleau sandstone sample (see **Table 1),** each of

them cylindrical in shape with 40 mm in length and 30 mm in diameter. The Icelandic samples were investigated in direct sequel to the electrical conductivity measurements performed by Kristinsdóttir et al. (2010). In the latter study, these samples were chosen to investigate the effect of different stages of alteration on the temperature dependence of electrical conductivity and the respective temperature coefficient; see Revil et al. (1998) and Kulenkampff et al. (2005) for definitions and Section 4 for details. In contrast, the Fontainebleau sample was only used in the present study as a reference material and was heated once to 150°C prior to the start of the experiment.

2.3. Fluids

As described in Kristinsdóttir et al. (2010), the samples were vacuum-saturated with the fluids before setting up the specimen assembly. This method also allowed to calculate the (connected) sample porosity; see Table 1. With the exception of sample K40 which was kept submerged within the in-situ fluid following drilling, the fluids used in specimens 2B, 3A, and 58 were synthetically prepared. This was done by dissolving reagent grade NaCl, KCl, Na_2SO_4, and K_2SO_4 salts in distilled water. The specific concentrations chosen were based on fluid analyses of samples taken at the respective well and reflect the principal in-situ chemical compositions, except for dissolved non-condensable gases. The resulting electrical fluid conductivities at 25°C are listed in Table 1. The fluid used for the Fontainebleau sandstone, as in previous studies (e.g. Milsch et al., 2008a), was a 0.1 molar NaCl standard solution having an electrical conductivity of 10.8 mS/cm at 25°C.

2.4. Experimental procedure

During the experiments both temperature T (nominally 150°C) and confining pressure (see Table 1) were kept constant while pore pressure was decreased to boil the pore fluid in a

199 controlled manner. The upstream pore fluid pump was stopped and the bypass valve (Fig. 1a)
200 was opened so that both sides of the sample were connected. The total volume of the pore
201 fluid system was steadily increased by retracting the downstream pore fluid pump at a
202 constant rate *r* (**Table 2**). As both sides of the sample were connected during this procedure,
203 the nominal pore pressure was equal at both faces of the specimen. The pore fluid pumps were
204 kept at room temperature and vaporization was restricted to the hot zone of the pore fluid
205 system located within the pressure vessel.
206 We emphasize that, in a procedure similar to experiments performed by Roberts et al.
207 (2001a), (1) we did work without a pressure gradient so that boiling was not restricted to one
208 end of the sample, (2) we did control the volume flow rate of the pump that was draining fluid
209 from the sample so that we had a measure of the volume of steam generated in the sample and
210 also of the resulting pore fluid pressure, and (3) we used a four-electrode arrangement to
211 measure the electrical properties with potential electrodes on the sample to eliminate electrode
212 and edge effects. During the experiments the electrical conductivity, the pore pressure, the
213 volume of the pore fluid pump, as well as the sample temperature were continuously
214 monitored.
215
216 **3. Results**
217
218 **Fig. 2** displays the raw experimental data as a function of time. The shaded area shows the
219 pressure range corresponding to the boiling point of water for the 145-150°C temperature
220 range. The pore fluid pumps that were used had a maximum pressure rating of 50 MPa. The
221 specifications report a resolution of ± 0.25 MPa and a zero pressure drift of ± 0.13 MPa in 48
222 hours at constant temperature. Due to these restrictions and in contrast to electrical
223 conductivity, the accuracy of determining the vapour pressure at a given temperature is
224 limited. Furthermore, fluctuations in sample temperature by up to ± 1°C and an apparently

225 correlated variation in pore pressure of 0.1-0.2 MPa/°C occurred at some stages of the
226 experiment. This was much greater than the almost linear 0.012 MPa/°C variation in pressure
227 that would be expected at the boiling point in the 145-150°C temperature range. In fact, these
228 temperature and pressure fluctuations are indirectly related to each other and represent
229 experimental artefacts that originate from laboratory temperature variations.

230 In previous experiments (e.g. Milsch et al., 2008a; 2008b) we noticed that changes in
231 sample temperature T as measured with the two PT-100 sensors mentioned in Section 2.1 are
232 related to a signal drift of the thermocouple actively controlling the heater whose electrical
233 connector is located outside the pressure vessel. Similarly, changes in pore pressure are a
234 consequence of an electronic drift of the pressure gauge, which is exposed to the atmosphere,
235 and do not represent the true situation within the pore space of the sample. In these
236 experiments we also observed that variations in laboratory temperature yielded a linear
237 relationship between the temperature changes ΔT within the pressure vessel and the erroneous
238 variation of the pressure gauge read-out p_{pore}. This effect had to be removed from the data to
239 reveal the true pore pressure variations in the course of an experiment. Consequently, we
240 applied a linear correction that relates the true temperature variations as measured within the
241 vessel to apparent changes in pore pressure:

242 $$p_{pore}(T) = p_{pore}(T_0) + k(T - T_0)\,, \tag{3}$$

243 where p_{pore}, T, T_0, and k are the pore pressure, sample temperature, reference temperature, and
244 some temperature constant, respectively.

245 The reference couple [$p_{pore}(T_0)$, T_0] refers to the particular point in the pressure graphs of
246 Fig. 2 where the pore pressure remained constant for the first time, indicating the onset of
247 boiling (Section 4). The reference pressure p_{pore} was then determined as the tabulated vapour
248 pressure corresponding to the reference temperature T_0 (e.g. Lemmon et al., 2005). The
249 temperature constant k was determined from significant short-time variations of both

250 temperature T and pore pressure p_{pore} that could unequivocally be attributed to changes in
251 laboratory temperature (e.g. sample 58 between 17.5 and 18.5 h). The values of k differed
252 slightly from one experiment to another; see Table 1.
253 The result of this correction is shown in **Fig. 3**, which displays the pore fluid pressure as a
254 function of time together with the observed electrical conductivity changes, the sample
255 temperature, and the fluid volume drained from the sample. The total electrical conductivity
256 decrease during vaporization was generally 1 to 2 orders of magnitude and thus significant.
257 Except for sample 58 where the measurement was terminated earlier, the electrical
258 conductivity ultimately reached a minimum. For sample 2B, the pronounced conductivity
259 increase after 85 h remains unexplained.
260 For better visibility and for documentation, **Fig. 4** displays the corrected pore pressure of
261 each sample as a function of the volume change within the pore fluid system. The graphs
262 illustrate that, for all samples, there was a discontinuous decrease in pore pressure. Initially, as
263 the volume of the pore fluid system is increased, the pressure dropped rapidly due to elastic
264 relaxation. Then, at the boiling point, an approximately constant pore pressure level was
265 maintained. Finally, the pore pressure started to decrease again. Both the volumetric onset and
266 the extent of this second pore pressure decrease were sample-dependent.
267

268 **4. Discussion**
269
270 In this section we will interpret the observed, sample-dependent electrical conductivity
271 (Fig. 3) and pore pressure (Fig. 4) patterns with respect to drained pore fluid volume, steam
272 saturation, and predominant conduction mechanism.
273 In our experiments, the fluid started to boil once the vapour pressure corresponding to the
274 highest temperature within the pore fluid system was reached. The fluid was then in a state of
275 liquid-steam equilibrium at constant pore pressure as long as liquid at that temperature

276 remained. The principal decrease in electrical sample conductivity did not occur
277 instantaneously after the boiling pressure was reached (Fig. 3). We attribute this delay to the
278 initial vaporization of the free water inside the pore fluid system, before the onset of
279 significant boiling in the sample. Sometimes (e.g. samples 3A, FTBS12, and eventually 2B), a
280 smaller and transient electrical conductivity decrease was observed, followed by a
281 conductivity plateau. This observation is consistent with two different interpretations, either
282 (A) it was related to fluid boiling in the internal tubing and end caps of the assembly that cuts
283 off the residual current through the outer fluid capillaries, or (B) it was related to pore fluid
284 vaporization within the sample above the upper potential electrode. Due to the variability of
285 this effect from sample to sample, interpretation (B) is more likely to be correct and the
286 occurrence or absence of a conductivity plateau can be attributed to slight variations in the
287 temperature gradient along the sample. When fluid was continuously drained from the
288 sample, ultimately, a progressive decrease in electrical sample conductivity followed until the
289 latter reached a distinct minimum (Fig. 3).
290 The decrease in pore pressure at later stages of each experiment (Fig. 4) can be explained
291 by (A) temperature gradients along the specimen, (B) variations in the pore radii of an
292 individual sample as described by Roberts et al. (2001a), and/or (C) expansion of steam after
293 all liquid at 150°C has been vaporized. With respect to (A), the minimum pore pressure
294 observed was approximately 0.2 MPa corresponding to a vaporization temperature of only
295 120°C, which is inconsistent with the experimental conditions. As long as there is liquid left
296 to vaporize and if the rate at which the volume of the pore fluid system is increased is low
297 enough so that the equilibrium pressure can be maintained by steam production - which
298 evidently was the case in all experiments (Fig. 4) - it is reasonable to inquire if the observed
299 decrease in pore pressure is because of a vapour pressure drop due to capillarity (case B).
300 The relationship between variations in both electrical conductivity and pore (vapour)

pressure with respect to the drained fluid volume was observed to be sample-dependent. Disparities in the pore pressure change pattern would then reflect differences in sample microstructure with respect to the distribution of individual pore radii; i.e.,

(I) For samples 2B, 3A, and FTBS12, the pore pressure started to decrease after the electrical conductivity had dropped by about 90 %, evidence of both large pores and a narrow pore radius distribution.

(II) For sample K40, the pore pressure started to decrease after the conductivity had dropped by approximately 50 %, indicating the predominance of one narrow pore size class larger than the remaining pores that have a broad pore radius distribution.

(III) For sample 58, both electrical conductivity and pore pressure initially showed a concurrent decrease followed by a continuous drop in conductivity at constant vapour pressure (Fig. 3, after 19 h). This suggests a broad pore radius distribution and the existence of one narrow class of smaller pores.

For the Fontainebleau sandstone interpretation (I) is in agreement with mercury porosimetry measurements performed by Milsch et al. (2008a). The pore radius distribution in this rock is very narrow, with 90 % of porosity accounted for by pores with radii between 4 to 10 μm. For the Icelandic samples these data are not yet available. However, if capillarity is solely responsible for the observed decrease in pore pressure, the above scenarios are consistent.

Following the procedure in Roberts et al. (2001a) we calculated the minimum pore (capillary) radius R related to vaporization by the maximum capillary pressure observed (p_{cap} $\approx$ 0.25 MPa at 150°C); we assumed a surface tension of the wetting fluid (water) of $5.2 \cdot 10^{-3}$ Pa•m (Weast, 1984) and a wetting angle of about zero. From Eq. (2) one obtains $R \geq 42$ nm, which indicates that virtually all pore size classes were affected by vaporization in the present experiments.

One important conclusion that can be drawn from the outcome of the experiments is the amount of drained fluid necessary to reduce the electrical conductivity to a minimum in relation to the individual sample porosity. To compare the electrical conductivity history of all samples as a function of the pump volume increase, we performed a conductivity normalization with respect to the starting values (Fig. 3); the results are shown in **Fig. 5**.

In all experiments 5 ± 1 ml of fluid had to be drained before the electrical conductivity of the sample became affected. This volume relates directly to the free fluid volume (e.g. in tubings) located inside the pressure vessel. The different starting values for volume change in Fig. 5 reflect the uncertainty in picking the correct sample related electrical conductivity decrease from Fig. 3. Except for sample 58, the observed conductivity patterns are similar. The electrical conductivity decreased to about 5 ± 1 % of its starting value. Furthermore (excluding sample 58), 7 ± 2 ml of fluid had to be drained from the sample until the minimum electrical conductivity was reached.

The (connected) pore volume between the potential electrodes was 2.2 (FTBS12), 2.3 (K40), 2.6 (2B), 3.5 (58), and 3.7 (3A) cm^3. The total (connected) pore volume of the samples was 3.5 (FTBS12), 3.7 (K40), 4.1 (2B), 5.7 (58), and 5.9 (3A) cm^3. Finally, the drained fluid volume at the conductivity minimum was approximately 5.1 (FTBS12), 9.2 (K40), 5.5 (2B), 17.7 (58), and 6.0 (3A) ml. The drained fluid volume for sample 58 follows from a linear extrapolation of the respective graph in Fig. 5.

As vaporization proceeded concurrently both between and outside the potential electrodes and fluid was drained from all parts of a sample, the ratio between the drained fluid volume and the pore volume is 1.5 (FTBS12), 2.5 (K40), 1.3 (2B), 3.1 (58), and 1.0 (3A), hence approximately 2.0 ± 1.0 times the relevant pore volume. Due to condensation outside the vessel the drained fluid volume in fact directly reflects the vaporized liquid volume contained within the pore space of a sample.

The ratio between the drained fluid volume and the total pore volume allows a classification of the rocks based on the normalized conductivity graphs in Fig. 5. Samples 3A, 2B, and FTBS12 display very similar conductivity patterns. Here, every part of the drained volume larger than the pore volume can be attributed to smaller pores and/or a broader pore size distribution as the excess volume reflects the vapour expansion related to a pressure decrease necessary for further vaporization. For example, 4.0 ml of fluid had to be drained from sample 3A to reduce the electrical conductivity by 90 % at constant pore pressure. Withdrawal of an additional 2.0 ml was necessary to attain the conductivity minimum by a concurrent decrease in pore pressure. For this sample, the drained fluid volume exceeded the total pore volume by only a small amount (0.1 ml). For sample 58, in contrast, the excess volume at the conductivity minimum was comparatively large. This suggests that the curve shapes in Fig. 5 could also be indicative of the respective dominant conduction mechanism as vaporization proceeds.

Electrical conduction in sample FTBS12 is definitely controlled by the pore fluid for the given fluid salinity (Milsch et al., 2008a). The same argument applied to samples 3A and 2B indicates that conduction during vaporization in hyaloclastites originating from the chlorite alteration zone should be controlled by the pore fluid as well, even for pore fluids of low salinity as those used in the present study. Sample K40, a basalt containing mixed-layer clays, displays a transition from pore fluid to surface conduction at a later vaporization stage. Finally and for the present fluid composition, conduction in sample 58, a basalt from the smectite alteration zone, is expected to be mainly surface controlled. In this case, the decrease in electrical conductivity upon continuous fluid drainage should be related to some progressive destruction of the conductive layer on the mineral surfaces rather than to the phase transformation within the pore space itself. Here, the correlation of electrical conductivity and pore pressure patterns is more complex; case (C) mentioned earlier. This

interpretation regarding differences in the predominant conduction mechanism for the present fluid-rock combinations is supported by a comparison of the conductivity temperature coefficients reported by Revil et al. (1998) with the ones measured by Kristinsdóttir et al. (2010): 0.023 1/°C for pore fluid conduction and 0.040 1/°C for interface conduction compared to 0.027 1/°C for samples 2B and 3A, 0.030 1/°C for sample K40, and 0.067 1/°C for sample 58, respectively.

A variety of conductivity models exist (e.g. Glover et al., 2000 and references therein) that extend Archie's Law (Archie, 1942) to more than one pore fluid phase. The correct application of such models requires the most probable distribution of the respective fluid phase to be known, which in the present study is very uncertain. However, if boiling occurs in thermodynamic equilibrium with the pore pressure decrease being controlled by capillarity, it is likely that vapour bubbles of progressively decreasing size are homogeneously distributed throughout the pore space of a sample. Taking sample FTBS12 as a reference, we conclude that at a maximum drained volume of approximately 1.5 times the pore volume, the free liquid contained within the pore space has been transformed into vapour. Consequently, for all samples where conduction is primarily related to the pore fluid, the electrical conductivity signal approximately reflects the respective liquid or steam saturation at a given stage of vaporization.

5. Conclusions

A high-pressure, high-temperature flow-through apparatus was used to perform electrical conductivity measurements under controlled *p-T* conditions during the water-steam phase transition in porous rocks from Icelandic hydrothermal reservoirs. In addition, one sample of Fontainebleau sandstone was studied as reference material.

The pore fluid vaporized at pressures equal to or below that of the boiling point of free

403 water at the respective temperature. After the onset of vaporization within the pore space, the
404 electrical conductivity of the samples decreased continuously by a factor of approximately 20
405 until reaching a distinct minimum.
406 For rocks with conduction primarily controlled by the pore fluid, the qualitative
407 application of the capillarity model proposed by Roberts et al. (2001a) yields a reasonable
408 interpretation of the observed concurrent variations of both electrical conductivity and pore
409 (vapour) pressure with respect to the pore size distribution. Based on the measured capillary
410 pressure, that model predicts that the decrease in electrical conductivity is associated with
411 boiling in virtually all pore size classes.
412 For two out of five samples, withdrawal of significant excess fluid volumes was necessary
413 to minimize electrical conductivity; thus implying that there is no direct relation between
414 conductivity, pore pressure and drained fluid volume in rocks where surface conduction
415 predominates. Therefore, it is concluded that the conduction mechanism controls the pattern
416 of electrical conductivity variations as vaporization proceeds.
417 The experimental results also suggest that, at the observed conductivity minimum, all
418 samples can be considered dry, apart from retained water on grain surfaces or in ultra-small
419 pores. Consequently, if the bulk conductivity of the rock is controlled by pore fluid
420 conduction, then changes in liquid-steam saturation can be characterized based on measured
421 changes in rock conductivity. Otherwise, if surface conduction predominates or if the
422 conduction mechanism is variable during vaporization, changes in steam saturation cannot be
423 quantified by conductivity measurements and the exact phase distribution of steam is
424 unknown.
425 In future investigations, priority should be given to studies that address: (1) the effect of
426 dissolved gases on conductivity during vaporization, as many geothermal reservoir fluids
427 contain significant amounts of gas, mainly CO_2, especially in the shallow parts of the

reservoir likely to develop a steam cap; (2) the quantitative relationship between the clay mineralogy and content and the conductivity patterns observed in the present study; and (3) the liquid-steam phase distribution within the pore space as boiling proceeds.

Acknowledgments

Steffi Meyhöfer and Rainer Becker, both at GFZ, are thanked for their technical support in the course of this study. We also thank Sabodh K. Garg, Marcelo J. Lippmann, William Cumming, Jeffery J. Roberts, and three anonymous reviewers for constructive comments that helped to improve the manuscript. This work is part of the I-GET Project and was supported by a grant from the 6th Framework Programme of the European Union.

References

Archie, G.E., 1942. The electrical resistivity log as aid in determining some reservoir characteristics. Trans. Am. Inst. Mech. Eng. 146, 54-61.

Atkinson, P.G., Pedersen, J.R., 1988. Using precision gravity data in geothermal reservoir engineering modeling studies. In: Procedings of the 13th Workshop on Geothermal Reservoir Engineering, Stanford University, Stanford, CA, USA, pp. 35–40.

Bear, J., 1988. Dynamics of fluids in porous media. Dover Publ., Inc. Mineola, NY, USA, 784 pp.

Boitnott, G.N., Hulen, J.B., 2001. Petrographic controls on electrical properties of core samples from the Awibengkok geothermal field, Indonesia. Geothermal Resources Council Trans. 25, 391-394.

Butler, D.B., Knight, R.J., 1995. The effect of steam quality on the electrical behavior of steam-flooded sands: A laboratory study. Geophysics 60, 998-1006.

Duba, A, Piwinskii, A.J., Santor, M., Weed, H.C., 1978. The electrical conductivity of

455 sandstone, limestone and granite. Geophysical Journal Royal Astronomical Society 53,
456 583-597.
457 Flóvenz, Ó.G., Georgsson, L.S., Árnason, K., 1985. Resistivity structure of the upper crust in
458 Iceland. J. Geophys. Res. 90(B12), 10136-10150.
459 Flóvenz, Ó.G., Spangenberg, E., Kulenkampff, J., Árnason, K., Karlsdóttir, R., Huenges, E.,
460 2005. The role of electrical interface conduction in geothermal exploration. In:
461 Procedings of the 2005 World Geothermal Congress, 24-30 April, Antalya, Turkey, 9
462 pp.
463 Glover, P.W.J., Hole, M.J., Pous, J., 2000. A modified Archie's law for two conducting phases.
464 Earth Planet. Sci. Lett. 180, 369-383.
465 Guéguen, Y., Palciauskas, V. 1994. Introduction to the physics of rocks. Princeton University
466 Press, Princeton, NJ, USA, 392 pp.
467 Hunt, T., Bowyer, D., 2007. Reinjection and gravity changes at Rotokawa geothermal field,
468 New Zealand. Geothermics 36, 421-435.
469 Kristinsdóttir, L.H., Flóvenz, Ó.G., Bruhn, D., Milsch, H., Spangenberg, E., 2007. Electrical
470 Conductivity and Sonic Velocity of Icelandic Rock Core Samples Measured at high
471 Temperature and Pressure. Technical report ÍSOR-2007/065, Iceland GeoSurvey,
472 Reykjavik, Iceland, 40 pp.
473 Kristinsdóttir, L.H., Flóvenz, Ó.G., Árnason, K., Bruhn, D., Milsch, H., Spangenberg, E.,
474 Kulenkampff, J., 2010. Laboratory measurements of conductivity of rock samples
475 from Icelandic high temperature geothermal fields as a function of temperature at in-
476 situ conditions. Geothermics (submitted manuscript).
477 Kulenkampff, J., Spangenberg, E., Flóvenz, Ó.G., Raab, S., Huenges, E., 2005. Petrophysical
478 parameters of rocks saturated with liquid water at high temperature geothermal
479 reservoir conditions. In: Proceedings of the 2005 World Geothermal Congress, 24-30

April, Antalya, Turkey, 9 pp.

Lemmon, E.W., McLinden, M.O., Friend, D.G., 2005. Thermophysical Properties of Fluid Systems. In: NIST Standard Reference Database 69, P.J. Linstrom and W.G. Mallard (Eds.), National Institute of Standards and Technology, Gaithersburg, MD, USA, http://webbook.nist.gov/chemistry/.

Milsch, H., Blöcher, G., Engelmann, S., 2008a. The relationship between hydraulic and electrical transport properties in sandstones: An experimental evaluation of several scaling models. Earth Planet. Sci. Lett. 275, 355-363, doi 10.1016/j.epsl.2008.08.031.

Milsch, H., Spangenberg, E., Kulenkampff, J., Meyhöfer, S., 2008b. A new apparatus for long-term petrophysical investigations on geothermal reservoir rocks at simulated in-situ conditions. Transport in Porous Media 74, 73-85, doi 10.1007/s11242-007-9186-4.

Nicholson, K., 1993. Geothermal Fluids - Chemistry and Techniques. Springer Verlag, Berlin, Germany, 263 pp.

Revil, A., Cathles III, L.M., Losh, S., 1998. Electrical conductivity in shaly sands with geophysical applications. J. Geophys. Res. 103 (B10), 23925-23936.

Rink, M., Schopper, J.R., 1976. Pore structure and physical properties in porous sedimentary rocks. Pure Applied Geophysics 114, 273-284.

Roberts, J. J., Bonner, B. P., Duba, A. G., 2000. Electrical resistivity measurements of andesite and hydrothermal breccia from the Awibengkok geothermal field, Indonesia. In: Proceedings of the 25th Workshop on Geothermal Reservoir Engineering, Stanford University, Stanford, CA, USA, pp. 339-341.

Roberts, J.J., Duba, A.G., Bonner, B.P., Kasameyer, P.W., 2001a. The effects of capillarity on electrical resistivity during boiling in metashale from scientific corehole SB-15-D, The Geysers, California, USA. Geothermics 30, 235-254.

505 Roberts, J.J., Bonner, B.P., Kasameyer, P.W., 2001b. Electrical resistivity measurements of
506 intact and fractured geothermal reservoir rocks. In: Proceedings of the 26th Workshop
507 on Geothermal Reservoir Engineering, Stanford University, Stanford, CA, USA, pp.
508 94-99.
509 Roberts, J.J., 2002. Electrical properties of microporous rock as a function of saturation and
510 temperature. Journal of Applied Physics 91, 1687-1694.
511 Ruffet, C., Darot, M., Guéguen, Y., 1995. Surface conductivity in rocks: A review. Surveys in
512 Geophys. 16, 83-105.
513 Vaughan, P.J., Udell, K.S., Wilt, M.J., 1993. The effects of steam injection on the electrical
514 conductivity of an unconsolidated sand saturated with a salt solution. J. Geophys. Res.
515 98 (B1), 509-518.
516 Weast, R.C. (Ed.), 1984. CRC Handbook of Chemistry and Physics, 64th Edition. CRC Press,
517 Boca Raton, FL, USA, 2386 pp.

518
519
520 **Figure captions**

521 **Fig. 1. (a)** General set-up of the experimental apparatus used in this study. (1) downstream
522 pore fluid pumps; (2) reservoirs for fluid sampling; (3) pressure vessel with internal heater
523 and specimen assembly; (4) confining pressure pump; (5) upstream pore fluid pumps; (6)
524 fluid reservoir. **(b)** Details of the mounted specimen assembly.

525

526 **Fig. 2**. Main results of the pore fluid vaporization experiments - raw data: Changes in
527 electrical conductivity (blue), temperature (red), volume in pore fluid pump (black) and pore
528 pressure (as measured in pump; green) with time. The shaded area shows the (vapour)
529 pressure at which water boils for T = 145-150°C. Note that there is a break in the pore
530 pressure axis for all graphs. In the plot labeled “Sample 3A (begin)”, only the first 30 hours of

the experiment are shown to highlight early time variations. See Section 3 for more details.

Fig. 3. Main results of the pore fluid vaporization experiments - pore pressure corrected according to Eq. (3): Changes in electrical conductivity (blue), temperature (red), volume in pore fluid pump (black) and pore pressure (as measured in pump; green) with time. The shaded area shows the (vapour) pressure at which water boils for T = 145-150°C. Note that there is a break in the pore pressure axis for all graphs. For sample 3A the first 30 hours of the experiment are highlighted in plot "Sample 3A (begin)". See Section 3 for more details.

Fig. 4. Corrected pore pressure (Eq. 3) as a function of the volume increase in the pore fluid system. The shaded area shows the (vapour) pressure at which water boils for T = 145-150°C. Note that there is a break in the pressure axis for all samples except sample 58. See Section 3 for more details.

Fig. 5. Normalized electrical conductivity as a function of the volume increase in the pore fluid system. For each sample, the conductivity normalization was performed using the respective starting conductivity immediately before the initiation of boiling within the pore space as determined from Fig. 3. See Section 4 for more details.

Figures

Figure 1a

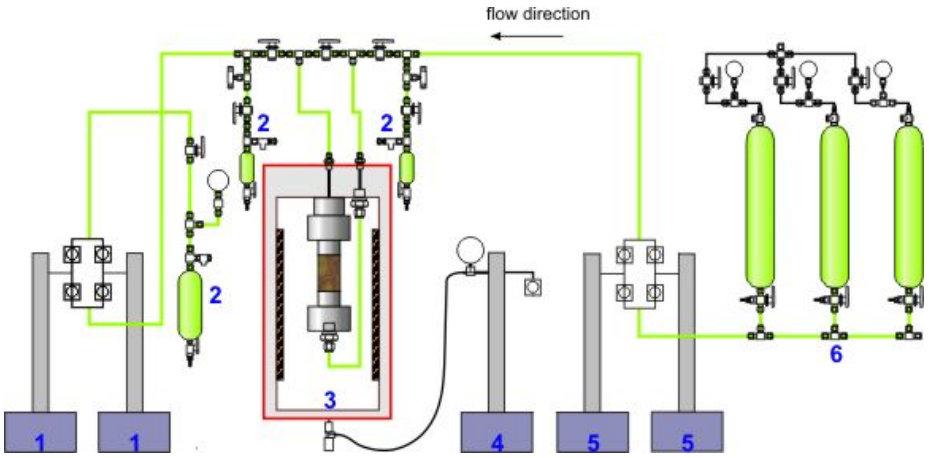

Figure 1b

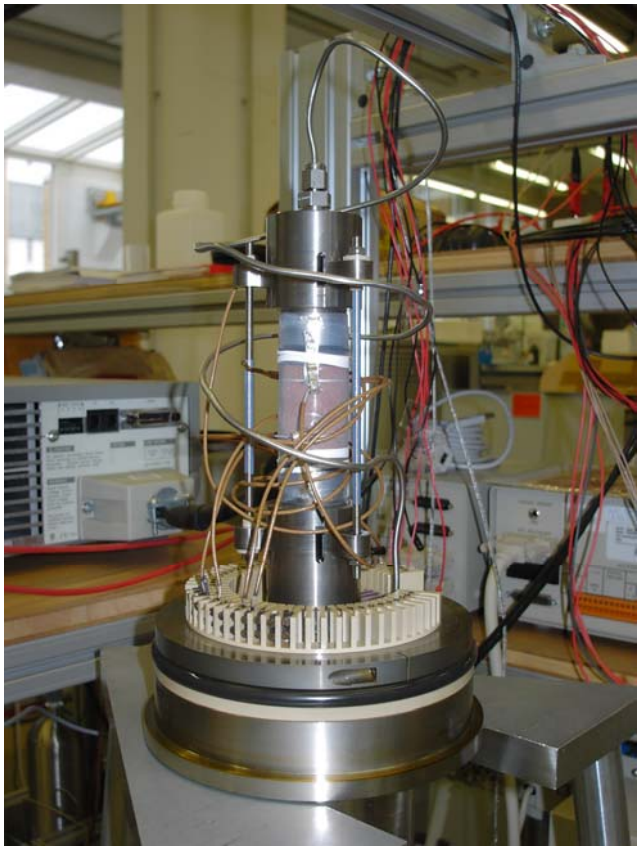

Figure 2

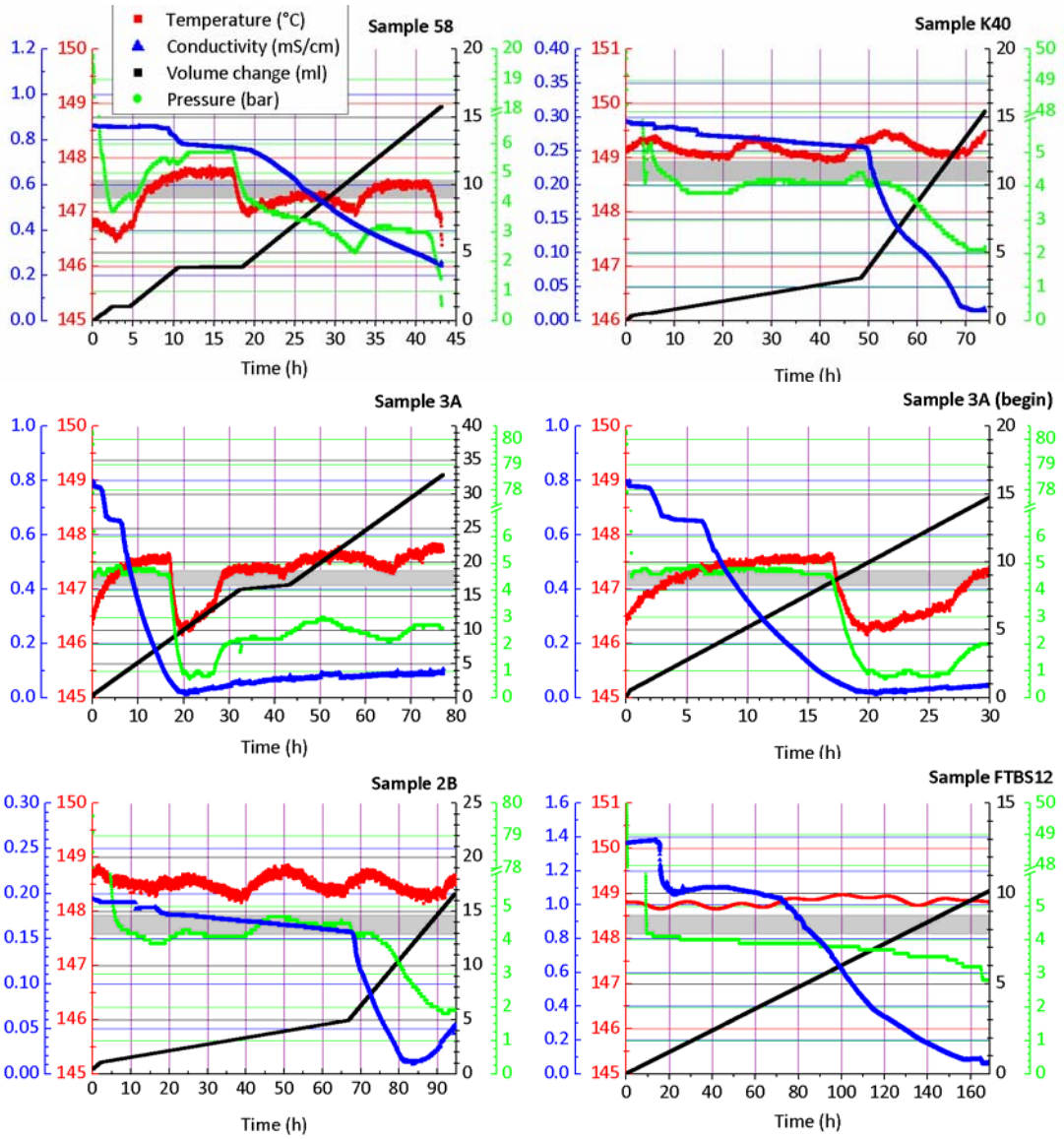
Temperature (°C)
Conductivity (mS/cm)
Volume change (ml)
Pressure (bar)
Sample 58
Sample K40
Sample 3A
Sample 3A (begin)
Sample 2B
Sample FTBS12
Time (h)

Figure 3

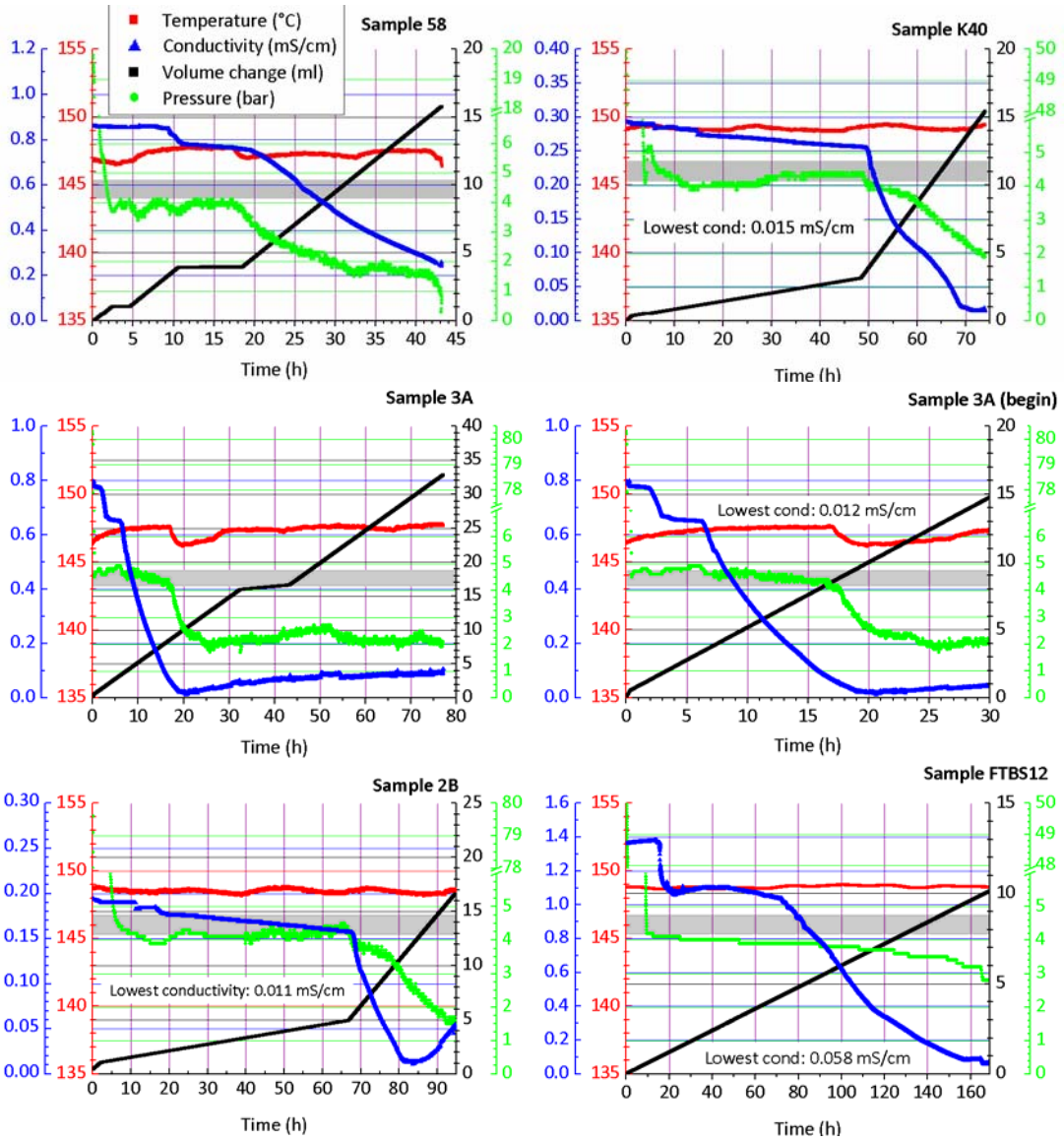
Temperature (°C)
Conductivity (mS/cm)
Volume change (ml)
Pressure (bar)
Sample 58
Time (h)
Sample K40
Lowest cond: 0.015 mS/cm
Time (h)
Sample 3A
Time (h)
Sample 3A (begin)
Lowest cond: 0.012 mS/cm
Time (h)
Sample 2B
Lowest conductivity: 0.011 mS/cm
Time (h)
Sample FTBS12
Lowest cond: 0.058 mS/cm
Time (h)

611 Figure 4
612
613

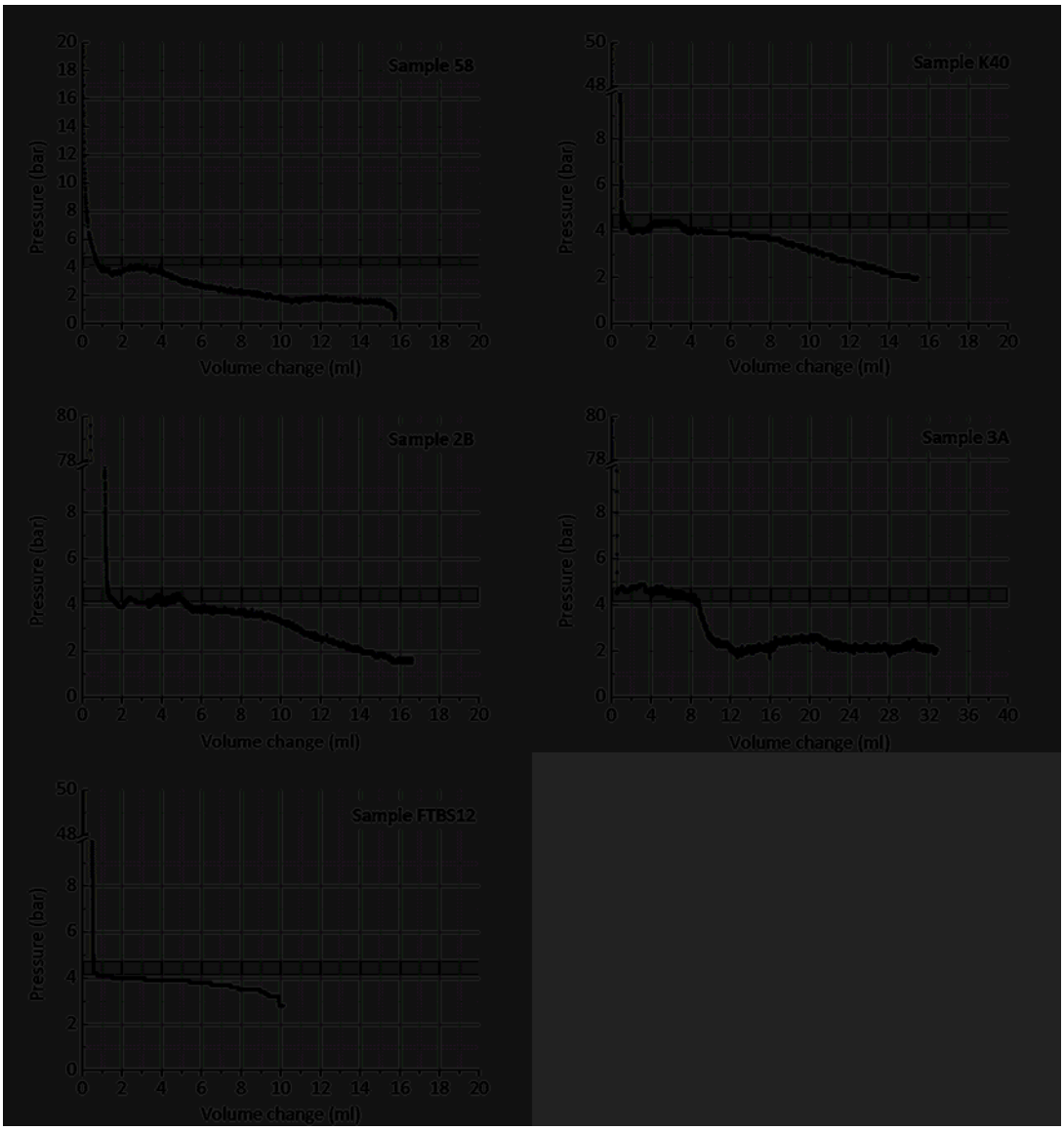

614
615
616
617 Figure 5
618

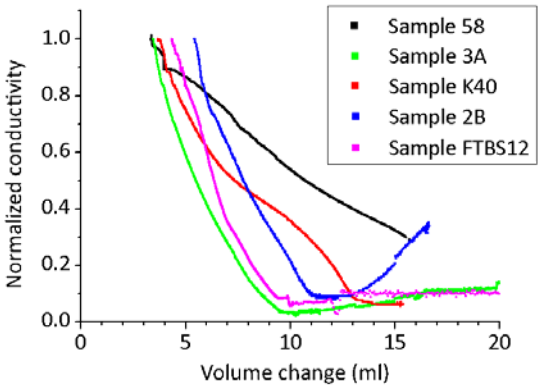

619

Tables

Table 1
Sample characteristics

Sample No.	Sampling location	Well No.	Year of sampling	Rock type	Hydrothermal alteration	Sample depth (m)	In-situ temperature (°C)	Estimated in-situ fluid conductivity at 25°C (mS/cm)	Porosity (%)	Density (g/cm^3)	Confining pressure (MPa)	Year of measurements	Temperature constant k (MPa/°C)
2B	Hengill	ÖJ-1	1994	Hyalo-clastite	Chlorite / Epidote	794.5	200	0.808	14.6	2.59	18.5	2007	0.10
3A	Hengill	ÖJ-1	1994	Hyalo-clastite	Chlorite / Epidote	795.0	200	0.808	20.7	2.46	15.0	2006	0.15
K40	Krafla	KH-5	2006	Basalt	MLC / Chlorite	537.5	120	---	13.2	2.29	13.5	2007	0.10
58	Krafla	KH-1	1991	Basalt	Smectite / MLC	187.5	~160	0.780	20.0	2.37	5.0	2006	0.15
FTBS12	Fontaine-bleau	N/A	2005	Sand-stone	None	(0)	(20)	(10.8)	12.5	2.29	10	2007	0

MLC: Mixed-layer clays

633 Table 2
634 Rate of volume increase *r* in the downstream pore fluid pump during vaporization
635
636
637

Sample No.	Rate of volume increase *r* (µl/min)	Time interval *t* (h)
2B	5	0 - 2
	1	2 - 67
	7	67 - 94.5
3A	25	0 - 0.3
	8	0.3 - 32.5
	1	32.5 - 43.5
	8	43.5 - 77
K40	5	0 - 1
	1	1 - 4
	0	4 - 5
	1	5 - 48.3
	8	48.3 - 74
58	8	0 - 4
	0	4 - 6.5
	8	6.5 - 10.5
	0	10.5 - 18.5
	8	18.5 - 43
FTBS12	1	0 - 169

638